materials

MDPI

Article

Green Synthesis of Silver-Decorated Magnetic Particles for Efficient and Reusable Antimicrobial Activity

Sachin V. Otari [1], Vipin Chandra Kalia [1], Aarti Bisht [1], In-Won Kim [1,2] and Jung-Kul Lee [1,*]

[1] Department of Chemical Engineering, Konkuk University, Seoul 05029, Korea; sachinotari169@gmail.com (S.V.O.); vckalia@gmail.com (V.C.K.); aartibisht94@gmail.com (A.B.); inwon@konkuk.ac.kr (I.-W.K.)
[2] Institute of SK-KU Biomaterials, Konkuk University, Seoul 05029, Korea
* Correspondence: jkrhee@konkuk.ac.kr; Tel.: +82-2-450-3505

Abstract: Metal and metal hybrid nanostructures have shown tremendous application in the biomedical and catalytic fields because of their plasmonic and catalytic properties. Here, a green and clean method was employed for the synthesis of silver nanoparticle (Ag NP)-SiO_2-Fe_2O_3 hybrid microstructures, and biomolecules from green tea extracts were used for constructing the hybrid structures. The SiO_2-Fe_2O_3 structures were synthesized using an ethanolic green tea leaf extract to form Bio-SiO_2-Fe_2O_3 ($BSiO_2$-Fe_2O_3) structures. Biochemical studies demonstrated the presence of green tea biomolecules in the $BSiO_2$ layer. Reduction of the silver ions was performed by a $BSiO_2$ layer to form Ag NPs of 5–10 nm in diameter in and on the $BSiO_2$-Fe_2O_3 microstructure. The reduction process was observed within 600 s, which is faster than that reported elsewhere. The antimicrobial activity of the Ag-$BSiO_2$-Fe_2O_3 hybrid structure was demonstrated against *Staphylococcus aureus* and *Escherichia coli*, and the nanostructures were further visualized using confocal laser scanning microscopy (CLSM). The magnetic properties of the Ag-$BSiO_2$-Fe_2O_3 hybrid structure were used for studying reusable antimicrobial activity. Thus, in this study, we provide a novel green route for the construction of a biomolecule-entrapped SiO_2-Fe_2O_3 structure and their use for the ultra-fast formation of Ag NPs to form antimicrobial active multifunctional hybrid structures.

Keywords: hybrid structure; green synthesis; antimicrobial activity

Citation: Otari, S.V.; Kalia, V.C.; Bisht, A.; Kim, I.-W.; Lee, J.-K. Green Synthesis of Silver-Decorated Magnetic Particles for Efficient and Reusable Antimicrobial Activity. *Materials* **2021**, *14*, 7893. https://doi.org/10.3390/ma14247893

Academic Editor: Ana Paula Piedade

Received: 2 November 2021
Accepted: 16 December 2021
Published: 20 December 2021

1. Introduction

For the last seven decades since the discovery of antibiotics, their uncontrolled use has led to a generation of antibiotic-resistant strains that are unresponsive to currently available conventional antibiotics, creating a major concern for the health sector [1,2]. More new-generation antibiotics have been introduced in the field of medicine; however, the toxicity and adverse effects of these antibiotics are worrying factors for implementation [3,4]. Therefore, alternate therapeutic strategies have been studied for the last two decades, and several types of nanomaterials have been tested for their antimicrobial activity that is nontoxic to human and nonhuman hosts [5–7]. Silver nanoparticles (Ag NPs) have been extensively studied because of their effective antimicrobial activity known since ancient times [8]. A detailed study of the antimicrobial activity of Ag NPs against a wide range of pathogenic microorganisms was performed; it was demonstrated that the Ag NPs act by releasing Ag+ ions, which act on bacteria through reactive oxygen species [8]. The antimicrobial activity of the Ag NPs decreases with aggregate formation, where Ag NPs form a bulky material that makes it difficult for them to act on small bacteria and viruses [9–11]. In addition, Ag NPs are not only toxic to the bacteria but also to mammalian cells, which is a major concern for the therapeutic use of Ag NPs [12]. Therefore, several functionalizations or immobilization procedures have been used to enhance their antimicrobial efficiency and avoid the aggregation and toxicity of Ag NPs before release into the environment [13]. Currently, extensive research is ongoing for the

construction of an ideal support to maintain the activity, stability, and reusability of Ag NPs [14].

Magnetic nanoparticles have been used as carriers for several nanomaterials, as they facilitate the separation of the nanoparticles by an external magnetic field and stability of the catalyst, which can reduce the adverse effects of the Ag NPs after use and reuse of Ag NPs for repeated applications [15]. Several researchers have demonstrated various methods for the synthesis of metal nanoparticle-supported SiO_2 NPs and magnetic nanoparticles; these methods are time-consuming and require hazardous materials and expensive instruments with harsh reaction procedures [16,17]. Ag@nanosilica NPs have been synthesized using a protein extract of *Rhizopus oryzae* after 72 h of incubation [18]. Kaloti et al. used glucose to form Ag–γ-Fe_2O_3 nanocomposites by applying a very high temperature [19]. Tzounis et al. used polyethyleneimine for the functionalization of SiO_2 nanospheres, wherein Ag NPs were decorated using sodium borohydride ($NaBH_4$) as the reducing agent [20]. Muthukumar et al. prepared silver ferrite nanoparticles from *A. blitum* leaf extract at 50 °C and pH 9 after 4 h of reaction time [21]. To the best of our knowledge, this is the first report where reducing molecules, i.e., plant leaf extract immobilized in the silica layer of silica-coated magnetic nanoparticles, were used for the reduction of Ag^+ ions to form metal-magnetic hybrid microstructures with ultrafine, spherical Ag NPs on the surface, within a short reaction duration and under mild reaction conditions. A major advantage of the hybrid structure synthesis method is the minimization of steps involving very complex, expensive, and cumbersome functionalization and reduction reaction conditions.

In this report, we present an economical and clean method for the construction of Ag-SiO_2-Fe_2O_3 hybrid structures by entrapping biomolecules from green tea leaf extract of *Camellia sinensis*, thus forming $BioSiO_2$ ($BSiO_2$)-Fe_2O_3 particles. The entrapped biomolecules reduced Ag^+ ions and formed Ag NPs on the $BSiO_2$-Fe_2O_3 particles. Different techniques were used for analyzing the crystal structure and morphology of the prepared hybrid structures, such as X-ray diffraction (XRD), high-resolution transmission electron microscopy (HR-TEM), and magnetic property measurement using a superconducting quantum interference device (SQUID). The prepared hybrid structures showed reusable active antimicrobial activity.

2. Materials and Methods

2.1. Materials

Analytical reagent-grade (AR-grade) chemicals were used for all experiments without purification. Silver nitrate ($AgNO_3$), iron (III) nitrate nonahydrate ($Fe(NO_3)_3{\cdot}9H_2O$), ethanol (C_2H_5OH; 99.9%), tetraethyl orthosilicate (TEOS), sodium carbonate, gallic acid monohydrate, 2,2-diphenyl-1-picrylhydrazyl (DPPH), 2,2′-azino-bis(3-ethylbenzothiazoline-6-sulphonic acid) (ABTS), potassium persulfate ($K_2Cr_2O_7$), and ammonium hydroxide (NH_4OH) were purchased from Sigma-Aldrich Co. Ltd. (St. Louis, MO, USA). Green tea bags (Jeju company, Korea) were purchased from the local market.

2.2. Preparation of the Ethanolic Extract of Green Tea Leaves

Green tea leaves (1.2 g) were ground and refluxed for 4 h in anhydrous ethyl alcohol (99.9%) under magnetic stirring. The suspension was cooled at room temperature and centrifuged at 4000 rpm for 10 min to remove large particulates of green tea leaves. Next, the green tea leaf extract was filtered through Whatman filter paper to remove small leaf particulates. Before further experimental procedures, the purified ethanolic green tea extract was kept in the dark at 4 °C.

2.3. Synthesis of Fe_2O_3 NPs

Fe_2O_3 NPs were synthesized using a previously reported method [22]. Briefly, 1 M of iron nitrate $Fe(NO_3)_3$ was prepared in 50 mL of distilled water (DW) under N_2 gas bubbling for 30 min. The pH of this solution was maintained at more than 10 under vigorous stirring by using aqueous ammonium hydroxide (30%). Then, the solution was

autoclaved at 150 °C for 10 h in a Teflon-lined stainless-steel reactor. The formed precipitate was centrifuged and washed several times with ethanol and water until a neutral pH was obtained. The particles were vacuum-dried at 50 °C for 12 h.

2.4. Synthesis of $BSiO_2$-Fe_2O_3 Particles

$BSiO_2$-Fe_2O_3 particles were synthesized using a previously reported method with modifications [23]. In the purified ethanolic green tea extract (40 mL), 50 mg of Fe_2O_3 NPs were dispersed under sonication for 20 min. Two milliliters of TEOS was added dropwise to the Fe_2O_3 NP suspension and further mixed with mechanical stirring for 1 h. The pH of the solution was adjusted to 11 by adding aqueous ammonium hydroxide dropwise. After 24 h of incubation, the formed particles were collected by centrifugation and repeatedly washed with ethanol and water. The $BSiO_2$-Fe_2O_3 particles were vacuum-dried at 50 °C for 12 h.

2.5. Synthesis of the Ag-$BSiO_2$-Fe_2O_3 Hybrid Microstructure

For the construction of the Ag-$BSiO_2$-Fe_2O_3 hybrid structure, the $BSiO_2$-Fe_2O_3 particles were dispersed in 10 mL of DW and sonicated for 20 min to disturb the agglomerates. Ten milliliters of aqueous $AgNO_3$ was poured into the solution to form a 10 mM $AgNO_3$ solution. The mixture was further incubated and stirred for 30 min and observed for color change. The formed hybrid structure was washed with water and ethanol several times, obtained with centrifugation, and vacuum-dried at 50 °C overnight.

2.6. Antimicrobial Activity

The antimicrobial activity of the Ag-$BSiO_2$-Fe_2O_3 hybrid microstructure was tested against *Staphylococcus aureus* and *Escherichia coli*. The growth media used for *S. aureus* and *E. coli* were trypticase soy broth and Luria–Bertani broth, respectively. The bacterial cultures were grown in the broths for 8 h to obtain the desired optical density (OD). Initially, the effect of the hybrid structure, streptomycin, AgNPs, and Fe_2O_3 NPs was tested on the growth curve of the bacterial cells for 22 h. The growth of both microorganisms was monitored using UV-visible spectroscopy, that is, optical density at 610 nm. Various concentrations of the hybrid structure, from 50 to 90 μg mL^{-1}, were added to the broths (10^6 to 10^7 bacterial cells mL^{-1}) and further incubated for 24 h at 37 °C. The antimicrobial activity of streptomycin, AgNPs, and Fe_2O_3 NPs was also studied with varied concentrations. After incubation, 0.1 mL from the incubated broth was spread over the respective agar and incubated for 24 h and observed for growth, and the colony-forming units (CFUs) mL^{-1} were measured. The higher concentrations of the hybrid nanostructure inhibited the growth of the bacteria completely, and they were used for the antimicrobial reusability experiment, in which 200 μg mL^{-1} of the hybrid structure was inoculated in 10^6 to 10^7 bacterial cells mL^{-1}. To visualize the antimicrobial activity of the prepared particles, a live/dead staining assay was performed after the exposure of 50 and 200 μg mL^{-1} of the nanohybrid nanostructure to *S. aureus* and *E. coli* cultures, as specified in earlier reports. The cells were observed under CLSM (Carl Zeiss LSM 710, Jena, Germany) [24].

2.7. Biochemical Analysis

2.7.1. Estimation of Total Phenolic Content

The total phenolic content of the green tea extract prepared using water and ethanol was determined using the McDonald method [25]. Briefly, a standard solution of gallic acid monohydrate (100 μg mL^{-1}) was prepared in methanol. Different concentrations of 0.1 to 1.0 mL of green tea leaf extract were mixed with a 1:1 mixture of Folin–Ciocalteu reagent and DW in 10 different tubes. To each tube, 7.5% sodium carbonate (2 mL) was added, and the mixture was allowed to react further for 30 min. The absorbance was measured at 765 nm, and the standard calibration curve was plotted. Then, 100 μL of the test samples was used to estimate the total phenolic content with a standard graph in terms of gallic acid equivalent (mg GAE g^{-1} extract).

2.7.2. DPPH Radical Scavenging Activity

The antioxidant properties of the ethanolic green tea extract and $BSiO_2$ NPs were measured based on the DPPH free radical scavenging activity [26]. In 100 mL of methanol, DPPH (6 mg) solution was prepared. The antioxidant activity was measured based on the discoloration of stable DPPH radicals in methanol, and at 517 nm, the absorbance was obtained. Different aliquots of the test samples were tested for the discoloration of DPPH solution. Using the given formula, the radical scavenging activity was calculated as follows: % Radical scavenging activity = absorbance (control) − absorbance (sample)/absorbance (control) × 100.

2.7.3. ABTS Radical Scavenging Assay

The ABTS radical scavenging assay was followed to demonstrate the antioxidant capability of the ethanolic green tea extract before and after TEOS hydrolysis by using a previously published method with some modifications [26]. Briefly, green tea extract and solution obtained from TEOS hydrolysis were diluted to different concentrations. They were added to 7 mM of ABTS standard solution prepared with 2.45 mM of potassium persulfate ($K_2S_2O_8$), and the mixture was further allowed to react for 6 min at 30 °C. After incubation, absorbance was measured at 734 nm. The radical scavenging activities of the extracts were calculated using the following equation and were compared with that of BHT: ABTS radical scavenging activity = absorbance (control) − absorbance (sample)/absorbance (control) × 100.

2.8. Analytical Instrumentation

UV-Visible spectroscopy was performed using a Schimadzu UV 1600 spectrophotometer with a 1 cm well-stoppered quartz cuvette. The morphology of the microstructures was evaluated by HR-TEM analysis using a JEM-3010 (JEOL) working at 300 kV and by energy-dispersive spectroscopy (EDS). Crystallography analysis of the nanostructures was performed using an X-ray diffractometer (Rigaku, Tokyo, Japan) with a Cu target. The magnetic properties of Fe_2O_3 and Fe_2O_3 hybrid structures were measured with a vibrating sample magnetometer (VSM; Lakeshore Cryotronics, Inc., Westerville, OH, USA). The antimicrobial activity was observed under CLSM. Dynamic light scattering (DLS) spectroscopy and zeta potential measurement of the particles in colloidal solution were performed using a NICOMP^{TM} 380 ZIS (Santa Barbara, CA, USA) for the determination of the hydrodynamic diameter (HDD) and charge on the particles.

3. Results and Discussion

3.1. Synthesis of the Hybrid Microstructure

The plant extract-mediated synthesis of nanomaterials has been one of the green chemistry approaches followed for the preparation of various materials. Extracts from several plant parts have been studied for the synthesis of metal nanoparticles that contain various polysaccharides, proteins, vitamins, or alkaloids, functionalizing and capping the nanomaterials with nontoxic and biodegradable biomaterials [27]. The presence of biomolecules on the surface of the nanoparticles leads to an increase in the colloidal stability of the nanoparticles forming a biomolecular corona on the surface, which contributes to enhanced bioactivity of the nanoparticles [28,29]. Here, in the presented work, the magnetic, catalytic active hybrid structure was synthesized with plant leaf extract biomolecules entrapped in SiO_2 on the surface of the magnetic nanostructure and further dispersed in aqueous Ag^+ ions for the reduction process to form Ag NPs on the $BSiO_2$-Fe_2O_3 particle surface. Table S1 provides the total phenolic content of green tea in water and ethanol. Though the phenolic content in ethanol compared to water was low, ethanol is the most favorable for the extraction of total phenols because it prevents the oxidation of phenolic compounds. In addition, the antioxidant property of the ethanolic and water extract, obtained from ABTS and DPPH scavenging assays, revealed effective antioxidant activity in both solvents. In alkaline ethanolic green tea extract, TEOS was added for the formation

of the SiO_2 layer, where the biomolecules present in the green tea extract become trapped, resulting in biomolecule-entrapped SiO_2 ($BSiO_2$) (Figure 1).

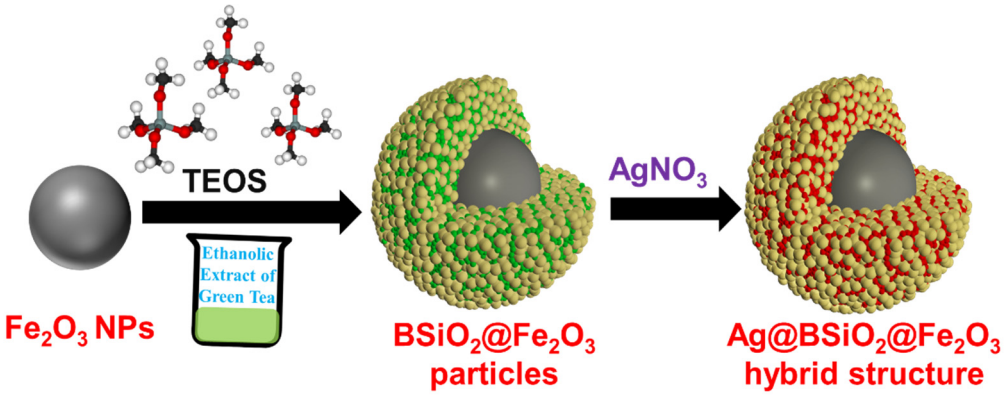

Figure 1. Schematics for the synthesis of silver-decorated biomolecule-entrapped SiO_2-coated Fe_2O_3 (Ag-$BSiO_2$-Fe_2O_3) hybrid structure.

The Fe_2O_3 NPs were synthesized using a previously reported hydrothermal method. Figure 2A,B show Fe_2O_3 NPs of an average diameter of 100 nm. To these magnetite NPs, the alkaline mixture of ethanolic green tea extract and TEOS was added and allowed to form the $BSiO_2$ layer on the surface of the Fe_2O_3 NPs for 12 h at room temperature. In Figure 2C,D, the smooth layer of $BSiO_2$ on the surface of the magnetite NPs can be observed to form a core–shell structure. The size of the magnetite NPs increased by approximately 30 nm, and a layer of 10–20 nm of $BSiO_2$ was formed. The formed core–shell structure was exposed to aqueous $AgNO_3$, and the active biomolecules of the $BSiO_2$ layer reduced $AgNO_3$ to form Ag NPs.

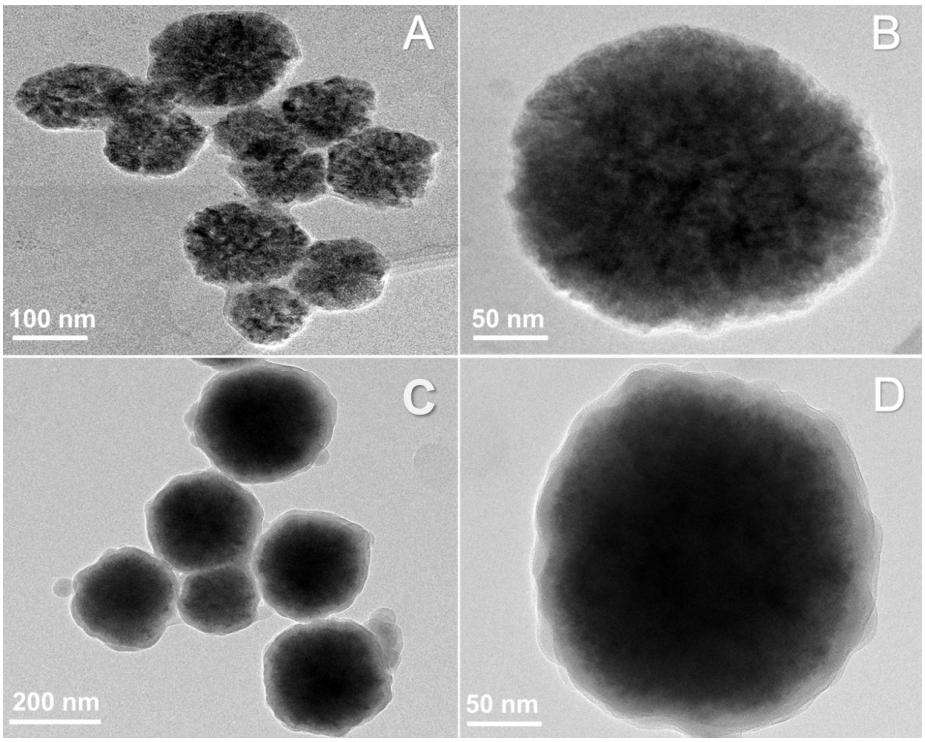

Figure 2. HR-TEM images of the (**A**,**B**) Fe_2O_3 nanosphere and (**C**,**D**) $BSiO_2$-Fe_2O_3 particles.

The synthesis of Ag NPs was confirmed using UV-visible spectroscopy (Figure 3A). No absorbance for Fe_2O_3 and $BSiO_2$-Fe_2O_3 NPs was observed in the range of 400–500 nm, whereas Ag-$BSiO_2$-Fe_2O_3 NPs showed characteristic absorbance at 424 nm, confirming the

formation of Ag NPs on the $BSiO_2$-Fe_2O_3 hybrid nanostructure. There are several reports on the synthesis of Ag NPs using biomaterials originating from plants and bacteria such as carbohydrates, amino acids, enzymes, proteins, and polyphenols [30]. Moulton et al. proposed a mechanism for the synthesis of Ag NPs using epigallocatechin-3-gallate obtained from *C. sinensis* leaf extract [31]. In addition, tea polyphenols, flavonoids, and epicatechin present in *C. sinensis* leaf extract were found to function as reducing and capping agents in the Ag NP synthesis process [31]. DFT calculations showed that the catechol moiety of flavonoids has a low energy of dissociation for the O–H bond of -OH groups, which is less than that of the -OH groups present in other parts of flavonoids [32]. The -OH groups of the catechol moiety of flavonoids have been demonstrated to function as metal-ion-reducing molecules. Various solvents have been utilized for the extraction of polyphenols and epicatechins from various plant extracts to maintain their high antioxidant activity [33]. Green tea extracts prepared in ethanol have high polyphenol content and retain high antioxidant properties [33]. Here, microhybrid structures were fabricated using the concentrated catechin derivatives from ethanolic green tea extract with active reducing capacity.

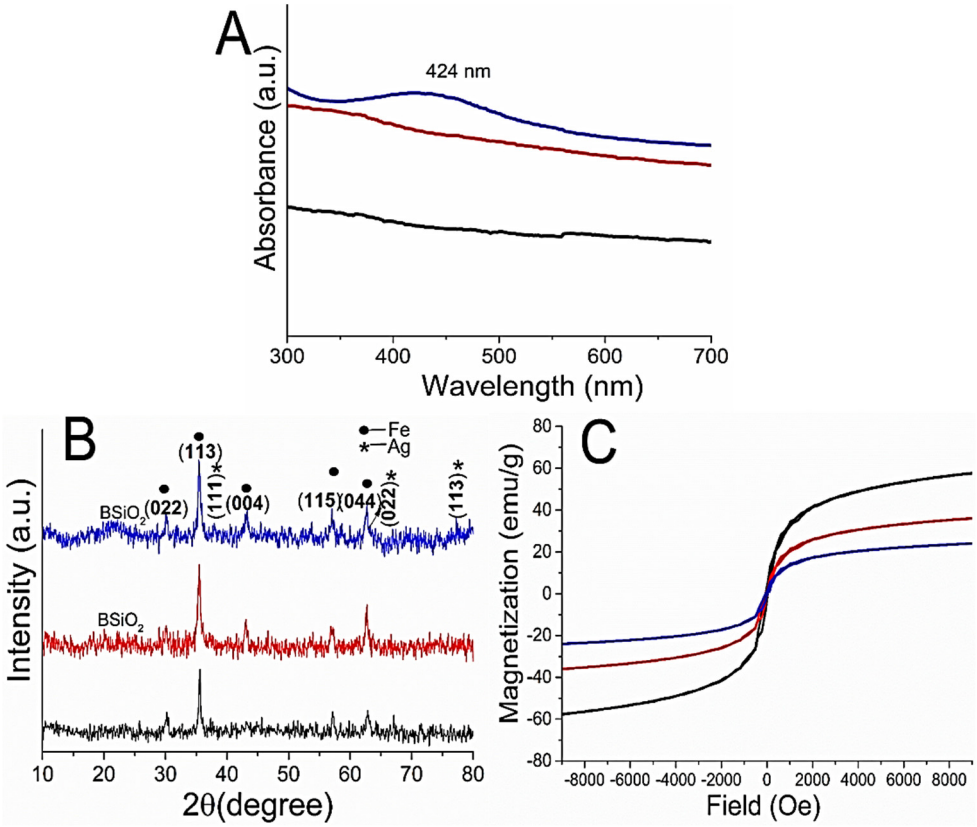

Figure 3. (**A**) UV-visible spectroscopic analysis of Fe_2O_3 NPs, $BSiO_2$-Fe_2O_3 particles, and Ag-$BSiO_2$-Fe_2O_3 structure. (**B**) XRD analysis. (**C**) Magnetization curves of γ-Fe_2O_3 NPs (black), $BSiO_2$-Fe_2O_3 particles (red), and Ag- $BSiO_2$-Fe_2O_3 structure (blue).

XRD spectra of the γ-Fe_2O_3 NPs (black), $BSiO_2$-Fe_2O_3 particles (red), and Ag-$BSiO_2$-Fe_2O_3 hybrid (blue) are shown in Figure 3B, demonstrating the crystallinity of the hybrid materials. The γ-Fe_2O_3 NPs showed a typical XRD pattern with the face-centered cubic structure of magnetite consistent with JCPDS card no. 96-101-3050 (Figure 3B, black). The characteristic peaks obtained at 2θ were 30.06°, 35.4°, 43.0°, 56.9°, and 62.5° and corresponded to (022), (113), (004), (115), and (044) indices, respectively [34]. The XRD data for $BSiO_2$-Fe_2O_3 particles (Figure 3B, red) were similar to those for Fe_2O_3 NPs, with a broad peak of 21° at 2θ corresponding to the amorphous $BSiO_2$ layer [20]. The XRD pattern of the Ag-$BSiO_2$-Fe_2O_3 hybrid (Figure 3B, blue) showed characteristic peaks for Fe_2O_3 along with characteristic peaks for Ag of 37.8°, 63.9°, and 76.7° at 2θ corresponding

to phase indices (111), (022), and (113), respectively (JCPDS card no. 969013048) [35]. The XRD pattern demonstrated the face-centered-cubic structure of metallic silver. A broad peak of 21–23° at 2θ for SiO_2 was observed in the XRD of the Ag-$BSiO_2$-Fe_2O_3 hybrid structure. The VSM measurement with a peak field of 20 KOe at room temperature was used to calculate the magnetic hysteresis loops of γ-Fe_2O_3 NPs (black), $BSiO_2$-Fe_2O_3 NPs (red), and Ag $BSiO_2$-Fe_2O_3 hybrid and to analyze changes in the magnetic behavior of the NPs with modifications (Figure 3C, blue). The saturation magnetization (M_s) value of the γ-Fe_2O_3 NPs was 61 emu g^{-1} at 300 K. After modification with $BSiO_2$ on the surface of the γ-Fe_2O_3 NPs, the saturation magnetization value reduced to 39 emu g^{-1}, and it further declined to 23 emu/g because of the presence of Ag NPs in the $BSiO_2$ layer. The decrease in the saturation magnetization may be due to the mass replacement and shielding of the magnetic NPs with SiO_2 and Ag NPs. The remanent magnetization (Mr) and coercivity (Hc) of the bare Fe_2O_3 were also affected by the modifications with SiO_2 and Ag NPs. The Mr decreased from 16.3 emu g^{-1} for γ-Fe_2O_3 NPs to 11.5 emu g^{-1} for $BSiO_2$-Fe_2O_3 NPs and then to 6.4 emu g^{-1} for the Ag-$BSiO_2$-Fe_2O_3 hybrid structure. The Hc value of Fe_2O_3 NP increased from 114 Oe to 121 Oe for the Ag-$BSiO_2$-Fe_2O_3 hybrid structure. The increase in Hc may be attributed to changes in the domain structure or surface coating anisotropy. Although the Ag-$BSiO_2$-Fe_2O_3 structure showed decreased saturation magnetization due to the presence of Ag NPs and SiO_2, it displayed extreme magnetic behavior, which suggests its magnetic separation capability. Thus, the Ag-$BSiO_2$-Fe_2O_3 nanohybrid can be recovered and reused by applying an external magnetic field. Therefore, the proposed method for modifying the SiO_2 nanostructures can be used for the construction of various hybrid nanostructures.

Figure 4A,B show HR-TEM images of the hybrid structure demonstrating the presence of small Ag NPs on the surface of the $BSiO_2$-Fe_2O_3 NPs, thus forming the Ag-$BsiO_2$-Fe_2O_3 hybrid structure. The Ag NPs were 5–10 nm in size and were distributed evenly in and on the $BsiO_2$ layer (Figure 4C). EDS analysis confirmed the presence of elemental silver in the hybrid nanostructure (Figure 4D). Figure 4E shows the elemental distribution of the Ag-$BSiO_2$-Fe_2O_3 structure displaying the elemental maps of C, Fe, O, Si, and Ag individually. The elemental mapping clearly shows that biomolecules from the green tea extracts were well distributed in the SiO_2 layer around the Fe_2O_3 nanoparticles, which further led to the synthesis of Ag NPs to form the hybrid nanostructure. The FT-IR spectrum of the extract of green tea and Ag-$BSiO_2$-Fe_2O_3 NPs with the spectral range from 400 to 4000 cm^{-1} showed the presence of bands at ~3327 cm^{-1}, ~2974 cm^{-1}, and 2880 cm^{-1}, corresponding to aliphatic OH groups, νCH_2, and C-H stretching, confirming the presence of phenolic compounds in green tea and Ag-$BSiO_2$-Fe_2O_3 NPs (Figure S1) [36]. The band at 1252 cm^{-1} corresponds to the vibrations of the C–O groups, which suggest the existence of polyols such as hydroxy flavonoids. The bands at 1044 cm^{-1} and 877 cm^{-1} correspond to CO stretching vibrations and C–C stretching vibrations, respectively, corresponding to the extract's flavonoids. The spectra of Ag-$BSiO_2$-Fe_2O_3 NPs at ~1074 cm^{-1} showed Si–O–Si stretching vibrations, confirming the presence of a SiO_2 layer on the Fe_2O_3 NPs [37].

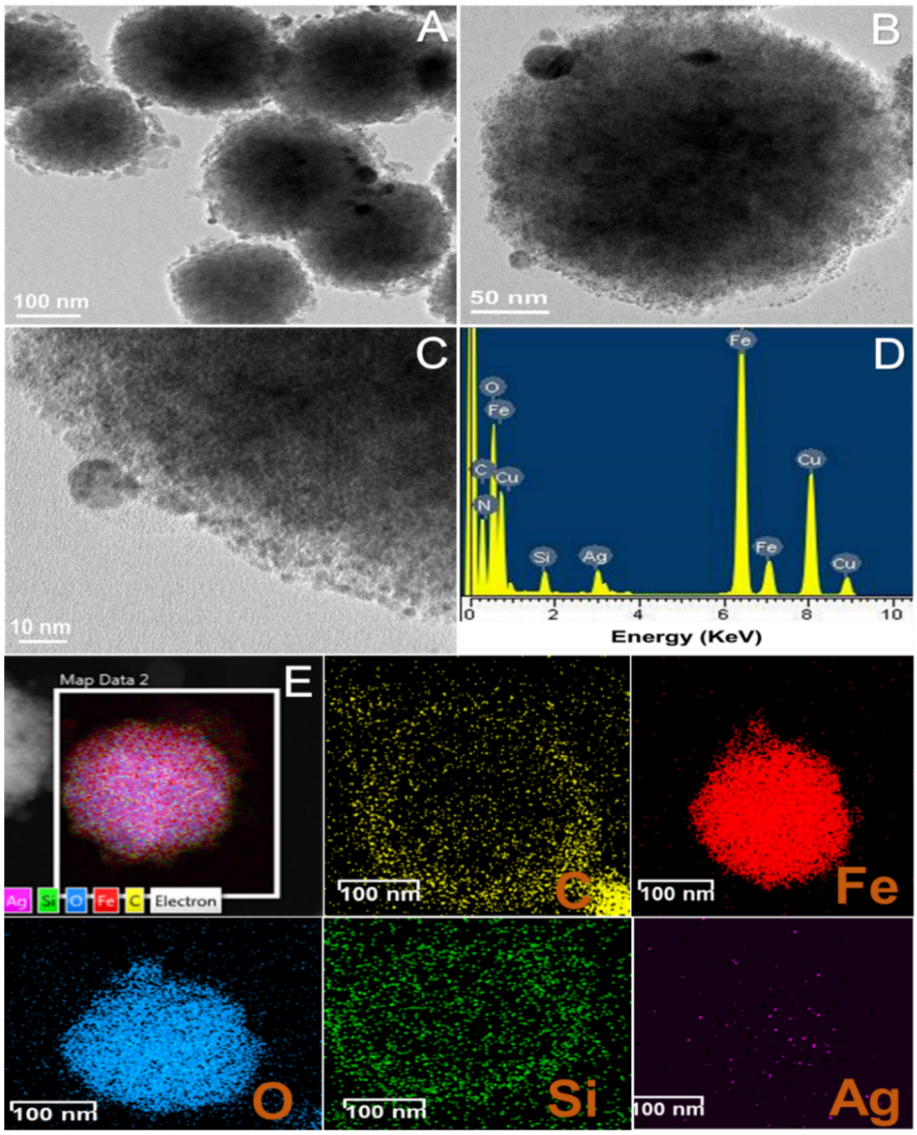

Figure 4. (**A**–**C**) HR-TEM images, (**D**) EDS spectrum analysis, and (**E**) elemental dot mapping of Ag-$BSiO_2$-Fe_2O_3 hybrid structure.

3.2. Antimicrobial Activity

The effective antimicrobial activity of the NPs is dependent on the NPs aggregation and interaction of the NPs with microbial cells. Thus, the hydrodynamic diameter (HDD) and zeta potential studies of the NPs provide information regarding the size and charge on the NPs in the colloidal solution, demonstrating the stability of NPs. The average HDD of the AgNPs, Fe_2O_3 NPs, and Ag-$BSiO_2$-Fe_2O_3 hybrid structure in the saline solution was 30 (Figure S2A), 200 (Figure S2B), and 500 nm (Figure S2C), respectively. The zeta potential of the AgNPs, Fe_2O_3 NPs, and Ag-$BSiO_2$-Fe_2O_3 hybrid structure was −28.6 (Figure S3A), −5.36 (Figure S3B), and −17.8 mV (Figure S3C), respectively. The antimicrobial activity of the streptomycin, AgNPs, Fe_2O_3 NPs, and Ag-$BSiO_2$-Fe_2O_3 hybrid structure was analyzed using *S. aureus* (Gram-positive) and *E. coli* (Gram-negative). The effective concentration of the various structures was determined by analyzing the inhibitory effect on the growth curve of both microorganisms; the time-dependent growth of the microorganisms was monitored at 610 nm. Figure 5 shows that 50 μg mL^{-1} of the microhybrid affected the growth rates of *S. aureus* (Figure 5A) and *E. coli* (Figure 5B), but it did not completely inhibit both microorganisms. At 100 and 200 μg mL^{-1}, the growth of both microorganisms was hampered, and no changes in the absorbance were observed after 20 h of incubation

with the Ag-$BSiO_2$-Fe_2O_3 structure. In similar experiments, a 10 μg mL^{-1} concentration of streptomycin and AgNPs showed an inhibitory effect on both microorganisms. The complete inhibition of *S. aureus* (Figure S4A) and *E. coli* (Figure S4B) was observed at 30 μg mL^{-1} of streptomycin, whereas 50 μg mL^{-1} of AgNPs showed complete inhibition of *S. aureus* (Figure S5A) and *E. coli* (Figure S5B). The Fe_2O_3 and $BSiO_2$-Fe_2O_3 NPs showed no effect on the bacterial growth curve in 50–200 μg mL^{-1} for both microorganisms (Figures S6 and S7). It is clear that 50 μg mL^{-1} of the hybrid structure was most effective for *S. aureus*, whereas *E. coli* showed some inhibition at this concentration. However, both microorganisms were highly sensitive to 200 μg mL^{-1} of the Ag-$BSiO_2$-Fe_2O_3 hybrid structure. To determine the minimum bactericidal concentration, both bacterial strains were exposed to various concentrations of the Ag-$BSiO_2$-Fe_2O_3 structure. Although 50 μg mL^{-1} of the hybrid structure reduced the growth of the microorganisms, it did not inhibit growth completely. However, as the concentration of the microhybrid increased from 50 to 90 μg mL^{-1}, the growth of both microorganisms constantly decreased. At 90 μg mL^{-1} of the hybrid structure, complete inhibition was observed for *S. aureus* (Figure 6A) and *E. coli* (Figure 6B); therefore, it can be considered the minimum bactericidal concentration (MBC) for both bacterial strains. For streptomycin, 20 μg mL^{-1} and 30 μg mL^{-1} were inhibitory for *S. aureus* and *E. coli*, respectively, as no growth was observed on growth plates (Figure S8). AgNPs inhibited both microorganisms at 30 μg mL^{-1} (Figure S9). However, the Fe_2O_3 and $BSiO_2$-Fe_2O_3 particles showed no effect on the microbial growth in 50 to 90 μg mL^{-1} (Figures S10 and S11). The AgNPs showed high stability and low HDD in the aqueous solution, which allowed the maximum interaction with microorganisms, leading to its effective antimicrobial activity, whereas the presence of plant extract and AgNPs on the surface Fe_2O_3 NPs increased the stability of the hybrid nanostructure compared to Fe_2O_3 NPs, allowing it to perform more effectively in antimicrobial activity. The CLSM study was performed to visualize the antimicrobial activity of the hybrid structure where a 200 μg mL^{-1} concentration of the hybrid structure is completely inhibitory to both species showing the red dead bacteria cells (Figures S12 and S13).

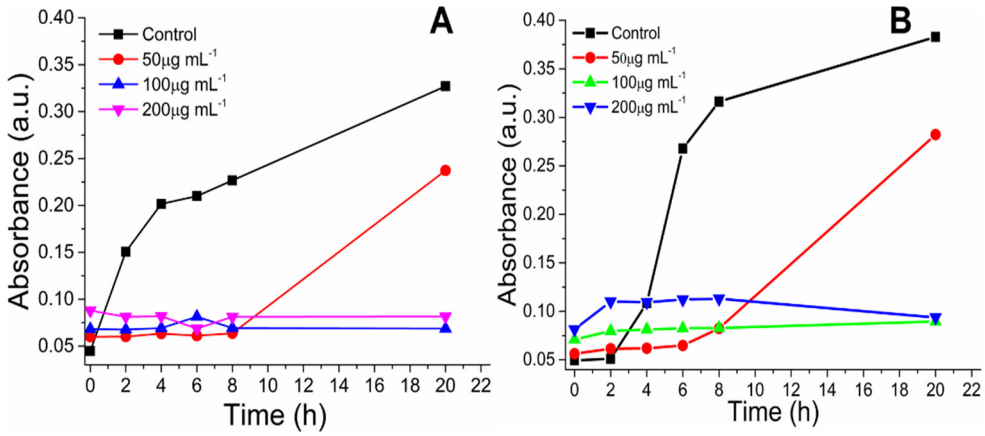

Figure 5. Growth curves of (**A**) *S. aureus* and (**B**) *E. coli* with various concentrations of the Ag-$BSiO_2$-Fe_2O_3 hybrid structure.

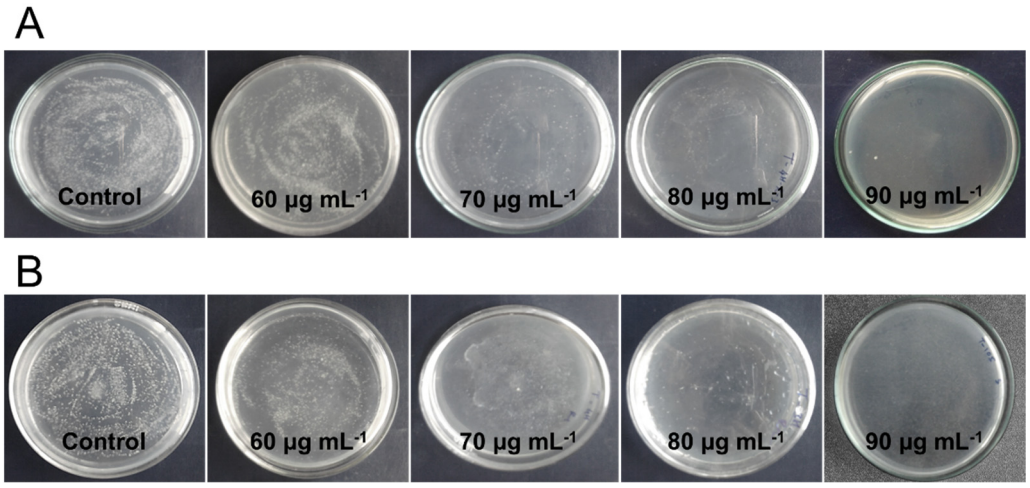

Figure 6. Growth plate photographs of (**A**) *S. aureus* and (**B**) *E. coli* with various concentrations of Ag-$BSiO_2$-Fe_2O_3 hybrid structure.

Because 200 µg mL^{-1} of the microhybrid caused complete inhibition of both pathogenic strains, the concentration of the hybrid structure was checked for repeated use of antimicrobial activity. The Ag-$BSiO_2$-Fe_2O_3 hybrid was added to each bacterial suspension, and the mixture was incubated for 24 h. After incubation, the hybrid material was isolated with an external magnet, and the bacterial suspension was analyzed spectroscopically. The hybrid structure was washed with a buffer before each repeated use, and the new bacterial suspension was added to this washed buffer. This was repeated for the next 5 cycles. The Ag-$BSiO_2$-Fe_2O_3 hybrid structure maintained 80% of its relative antimicrobial activity against *S. aureus* and 75% against *E. coli* (Figure 7). The loss of antimicrobial activity of the Ag-$BSiO_2$-Fe_2O_3 hybrid structure may be due to the loss of the hybrid material during isolation from the bacterial suspension.

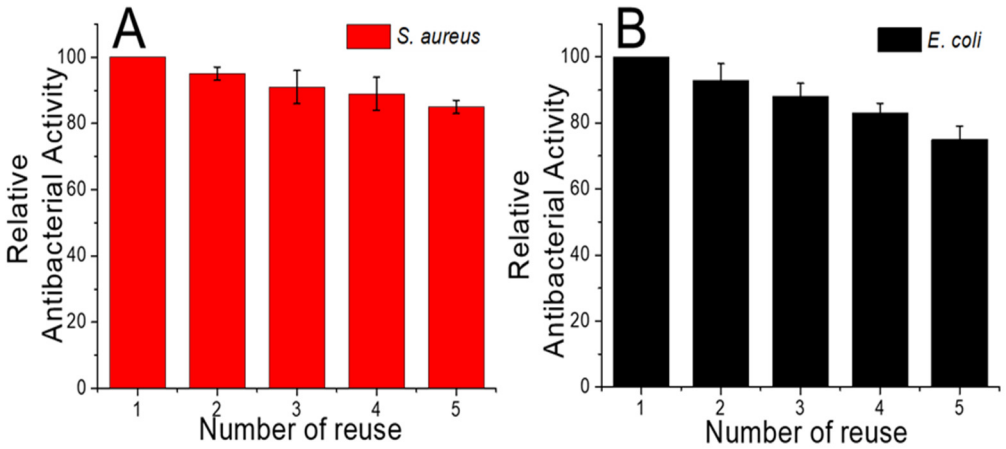

Figure 7. Reusable antibacterial effects of Ag-$BSiO_2$-Fe_2O_3 hybrid structure (200 µg mL^{-1}) on (**A**) *S. aureus* and (**B**) *E. coli*.

4. Conclusions

Here, we have developed a prominent, clean, robust method for the synthesis of an antimicrobial hybrid nanostructure using green tea active biomolecules. *C. sinensis* green tea ethanolic extract comprises polyphenols and other active ingredients and has a high antioxidant and reducing activity. The extract was allowed to become trapped in the SiO_2 layer by hydrolysis. This process of entrapment was employed to synthesize the separable SiO_2-coated Fe_2O_3 NPs magnetically. The reducing capacity of biomolecule-entrapped

SiO_2-Fe_2O_3 NPs was used to synthesize Ag NPs on the surface of the magnetic structure, thus forming the Ag-$BSiO_2$-Fe_2O_3 hybrid nanostructure. As the entrapped biomolecules have a high reducing capacity, the reduction of Ag^+ ions occurred quickly, which led to the formation of spherical Ag NPs with diameters in the range of 5–10 nm on the magnetic nanostructure. Elemental dot mapping revealed the uniform distribution of biomolecules and Ag NPs in the SiO_2 layer coated on Fe_2O_3 NPs. The Ag-$BSiO_2$-Fe_2O_3 hybrid microstructure showed excellent antimicrobial activity against *S. aureus* and *E. coli*. As the hybrid nanostructure was magnetic in nature, it showed excellent reusable antimicrobial activity. Toxicology studies need to be performed to use the antioxidant hybrid structure for medicinal and environmental applications. The outcome of the presented work creates opportunities for the construction of various metal microhybrid structures using eco-friendly biomaterials.

Supplementary Materials: The following are available online at https://www.mdpi.com/article/10.3390/ma14247893/s1, Figure S1: FT-IR spectroscopy analysis of green tea extract and Ag-$BSiO_2$ NPs-Fe_2O_3 NPs; Figure, S2: The Dynamic light scattering (DLS) analysis of colloids suspension of (A) Ag NPs, (B) Fe_2O_3 NPs, and (C) Ag-$BSiO_2$- Fe_2O_3 NPs; Figure S3: The zeta potential analysis of colloids suspension of (A) Ag NPs, (B) Fe_2O_3 NPs, and (C) Ag-$BSiO_2$- Fe_2O_3 NPs; Figure S4: Growth curves of (A) *S. aureus* and (B) *E. coli* with various concentrations of the streptomycin antibiotics; Figure S5: Growth curves of (A) *S. aureus* and (B) *E. coli* with various concentrations of the AgNPs; Figure S6: Growth curves of (A) *S. aureus* and (B) *E. coli* with various concentrations of the Fe_2O_3 NPs; Figure S7: Growth curves of (A) *S. aureus* and (B) *E. coli* with various concentrations of the $BSiO_2$-Fe_2O_3 NPs; Figure S8: Growth plate photographs of (A) *S. aureus* and (B) *E. coli* with various concentrations of streptomycin antibiotics; Figure S9: Growth plate photographs of (A) *S. aureus* and (B) *E. coli* with various concentrations of Ag NPs; Figure S10: Growth plate photographs of (A) *S. aureus* and (B) *E. coli* with various concentrations of Fe_2O_3 NPs; Figure S11: Growth plate photographs of (A) *S. aureus* and (B) *E. coli* with various concentrations of $BSiO_2$-Fe_2O_3 NPs; Figure S12: CLSM microscopy images of the antimicrobial activity of Ag-$BSiO_2$-Fe_3O_4 nanoparticles against *E. coli*.; Figure S13: CLSM microscopy images of the antimicrobial activity of Ag-$BSiO_2$-Fe_3O_4 nanoparticles against *S. aureus*. Table S1: Total phenolic contents and antioxidant activity of the green tea extract in different solvents.

Author Contributions: Conceptualization, S.V.O. and J.-K.L.; methodology, S.V.O. and A.B.; software, S.V.O.; validation, V.C.K., I.-W.K. and J.-K.L.; formal analysis, V.C.K.; investigation, S.V.O.; resources, S.V.O., A.B. and J.-K.L.; data curation, V.C.K.; writing—original draft preparation, S.V.O.; writing—review and editing, S.V.O., A.B. and J.-K.L.; visualization, V.C.K. and J.-K.L.; supervision, J.-K.L.; project administration, I.-W.K. and J.-K.L.; funding acquisition, J.-K.L. All authors have read and agreed to the published version of the manuscript.

Funding: This research received no external funding.

Institutional Review Board Statement: Not applicable.

Informed Consent Statement: Not applicable.

Data Availability Statement: Not applicable.

Acknowledgments: This work was supported by Konkuk University in 2019.

Conflicts of Interest: The authors declare no conflict of interest.

References

1. Tenover, F.C. Mechanisms of antimicrobial resistance in bacteria. *Am. J. Infect. Med.* **2006**, *119*, S3–S10. [CrossRef] [PubMed]
2. Holmes, A.H.; Moore, L.S.P.; Sundsfjord, A.; Steinbakk, M.; Regmi, S.; Karkey, A.; Guerin, P.J.; Piddock, L.J.V. Understanding the mechanisms and drivers of antimicrobial resistance. *Lancet* **2016**, *387*, 176–187. [CrossRef]
3. Kim, H.U.; Blin, K.; Lee, S.Y.; Weber, T. Recent development of computational resources for new antibiotics discovery. *Curr. Opin. Microbiol.* **2017**, *39*, 113–120. [CrossRef] [PubMed]
4. Gupta, A.; Mumtaz, S.; Li, C.H.; Hussain, I.; Rotello, V.M. Combatting antibiotic-resistant bacteria using nanomaterials. *Chem. Soc. Rev.* **2019**, *48*, 415–427. [CrossRef] [PubMed]
5. Hemeg, H.A. Nanomaterials for alternative antibacterial therapy. *Int. J. Nanomed.* **2017**, *12*, 8211–8225. [CrossRef] [PubMed]

6. Bandow, J.E.; Metzler-Nolte, N. New ways of killing the beast: Prospects for inorganic-organic hybrid nanomaterials as antibacterial agents. *ChemBioChem* **2009**, *10*, 2847–2850. [CrossRef] [PubMed]
7. Yacoby, I.; Benhar, I. Antibacterial nanomedicine. *Antibact. Nanomed.* **2008**, *3*, 329–341. [CrossRef]
8. Rai, M.; Yadav, A.; Gade, A. Silver nanoparticles as a new generation of antimicrobials. *Biotechnol. Adv.* **2009**, *27*, 76–83. [CrossRef]
9. Otari, S.V.; Patil, R.M.; Nadaf, N.H.; Ghosh, S.J.; Pawar, S.H. Green biosynthesis of silver nanoparticles from an actinobacteria *Rhodococcus* sp. *Mater. Lett.* **2012**, *72*, 92–94. [CrossRef]
10. Lok, C.N.; Ho, C.M.; Chen, R.; He, Q.Y.; Yu, W.Y.; Sun, H.; Tam, P.K.H.; Chiu, J.F.; Che, C.M. Silver nanoparticles: Partial oxidation and antibacterial activities. *JBIC J. Biol. Inorg. Chem.* **2007**, *12*, 527–534. [CrossRef] [PubMed]
11. Choi, O.; Deng, K.K.; Kim, N.J.; Ross, L.; Surampalli, R.Y.; Hu, Z. The inhibitory effects of silver nanoparticles, silver ions, and silver chloride colloids on microbial growth. *Water Res.* **2008**, *42*, 3066–3074. [CrossRef] [PubMed]
12. Ahamed, M.; AlSalhi, M.S.; Siddiqui, M.K.J. Silver nanoparticle applications and human health. *Clin. Chim. Acta* **2010**, *411*, 1841–1848. [CrossRef]
13. Wu, F.; Harper, B.J.; Harper, S.L. Differential dissolution and toxicity of surface functionalized silver nanoparticles in small-scale microcosms: Impacts of community complexity. *Environ. Sci. Nano* **2017**, *4*, 359–372. [CrossRef]
14. Zhao, X.S.; Bao, X.Y.; Guo, W.; Lee, F.Y. Immobilizing catalysts on porous materials. *Mater. Today* **2006**, *9*, 32–39. [CrossRef]
15. Dalpozzo, R. Magnetic nanoparticle supports for asymmetric catalysts. *Green Chem.* **2015**, *17*, 3671–3686. [CrossRef]
16. Tzounis, L.; Logothetidis, S. Fe_3O_4@SiO_2 core shell particles as platforms for the decoration of Ag nanoparticles. *Mater. Today Proc.* **2017**, *4*, 7076–7082. [CrossRef]
17. Sui, N.; Monnier, V.; Salvia, M.V.; Chevolot, Y.; Souteyrand, E. Magnetic and optical properties of Ag@SiO_2-FITC-Fe_3O_4 hybrid nanoparticles. *Mater. Sci. Eng. B* **2014**, *182*, 92–95. [CrossRef]
18. Das, S.K.; Khan, M.M.R.; Parandhaman, T.; Laffir, F.; Guha, A.K.; Sekaran, G.; Mandal, A.B. Nano-silica fabricated with silver nanoparticles: Antifouling adsorbent for efficient dye removal, effective water disinfection and biofouling control. *Nanoscale* **2013**, *5*, 5549–5560. [CrossRef]
19. Kaloti, M.; Kumar, A.; Navani, N.K. Synthesis of glucose-mediated Ag-γ-Fe_2O_3 multifunctional nanocomposites in aqueous medium—A kinetic analysis of their catalytic activity for 4-nitrophenol reduction. *Green Chem.* **2015**, *17*, 4786–4799. [CrossRef]
20. Tzounis, L.; Contreras-Caceres, R.; Schellkopf, L.; Jehnichen, D.; Fischer, D.; Cai, C.; Uhlmann, P.; Stamm, M. Controlled growth of Ag nanoparticles decorated onto the surface of SiO2 spheres: A nanohybrid system with combined SERS and catalytic properties. *RSC Adv.* **2014**, *4*, 17846–17855. [CrossRef]
21. Muthukumar, H.; Palanirajan, S.K.; Shanmugam, M.K.; Gummadi, S.N. Plant extract mediated synthesis enhanced the functional properties of silver ferrite nanoparticles over chemical mediated synthesis. *Biotechnol. Rep.* **2020**, *26*, e00469. [CrossRef]
22. Darezereshki, E. Synthesis of maghemite (γ-Fe_2O_3) nanoparticles by wet chemical method at room temperature. *Mater. Lett.* **2010**, *64*, 1471–1472. [CrossRef]
23. Deng, Y.H.; Wang, C.C.; Hu, J.H.; Yang, W.L.; Fu, S.K. Investigation of formation of silica-coated magnetite nanoparticles via sol-gel approach. *Colloids Surf. A Physicochem. Eng. Asp.* **2005**, *262*, 87–93. [CrossRef]
24. Chaurasia, A.K.; Thorat, N.D.; Tandon, A.; Kim, J.H.; Park, S.H.; Kim, K.K. Coupling of radiofrequency with magnetic nanoparticles treatment as an alternative physical antibacterial strategy against multiple drug resistant bacteria. *Sci. Rep.* **2016**, *6*, 33662. [CrossRef]
25. de Oliveira, A.C.; Valentim, I.B.; Silva, C.A.; Bechara, E.J.H.; de Barros, M.P.; Mano, C.M.; Goulart, M.O.F. Total phenolic content and free radical scavenging activities of methanolic extract powders of tropical fruit residues. *Food Chem.* **2009**, *115*, 469–475. [CrossRef]
26. Ahmed, S.; Ahmad, M.; Swami, B.L.; Ikram, S. A review on plants extract mediated synthesis of silver nanoparticles for antimicrobial applications: A green expertise. *J. Adv. Res.* **2016**, *7*, 17–28. [CrossRef]
27. Rónavári, A.; Kovács, D.; Igaz, N.; Vágvölgyi, C.; Boros, I.M.; Kónya, Z.; Pfeiffer, I.; Kiricsi, M. Biological activity of green-synthesized silver nanoparticles depends on the applied natural extracts: A comprehensive study. *Int. J. Nanomed.* **2017**, *12*, 871–883. [CrossRef]
28. Rónavári, A.; Bélteky, P.; Boka, E.; Zakupszky, D.; Igaz, N.; Szerencsés, B.; Pfeiffer, I.; Kónya, Z.; Kiricsi, M. Polyvinyl-pyrrolidone-coated silver nanoparticles—The colloidal, chemical and biological consequences of steric stabilization under biorelevant conditions. *Int. J. Mol. Sci.* **2021**, *22*, 8673. [CrossRef] [PubMed]
29. Bélteky, P.; Rónavári, A.; Igaz, N.; Szerencsés, B.; Tóth, I.Y.; Pfeiffer, I.; Kiricsi, M.; Kónya, Z. Silver nanoparticles: Aggregation behavior in biorelevant conditions and its impact on biological activity. *Int. J. Nanomed.* **2019**, *14*, 667–687. [CrossRef]
30. Hussain, S.; Khan, Z. Epigallocatechin-3-gallate-capped Ag nanoparticles: Preparation and characterization. *Bioprocess Biosyst. Eng.* **2014**, *37*, 1221–1231. [CrossRef] [PubMed]
31. Moulton, M.C.; Braydich-Stolle, L.K.; Nadagouda, M.N.; Kunzelman, S.; Hussain, S.M.; Varma, R.S. Synthesis, characterization and biocompatibility of "green" synthesized silver nanoparticles using tea polyphenols. *Nanoscale* **2010**, *2*, 763–770. [CrossRef] [PubMed]
32. Trouillas, P.; Marsal, P.; Siri, D.; Lazzaroni, R.; Duroux, J.L. A DFT study of the reactivity of OH groups in quercetin and taxifolin antioxidants: The specificity of the 3-OH site. *Food Chem.* **2006**, *97*, 679–688. [CrossRef]
33. Navale, S.T.; Bandgar, D.K.; Nalage, S.R.; Khuspe, G.D.; Chougule, M.A.; Kolekar, Y.D.; Sen, S.; Patil, V.B. Synthesis of Fe2O3 nanoparticles for nitrogen dioxide gas sensing applications. *Ceram. Int.* **2013**, *39*, 6453–6460. [CrossRef]

34. Otari, S.V.; Patil, R.M.; Waghmare, S.R.; Ghosh, S.J.; Pawar, S.H. A novel microbial synthesis of catalytically active Ag-alginate biohydrogel and its antimicrobial activity. *Dalton Trans.* **2013**, *42*, 9966–9975. [CrossRef] [PubMed]
35. Shin, K.S.; Cho, Y.K.; Choi, J.-Y.; Kim, K. Facile synthesis of silver-deposited silanized magnetite nanoparticles and their application for catalytic reduction of nitrophenols. *Appl. Catal. A Gen.* **2012**, *413–414*, 170–175. [CrossRef]
36. Yi, T.; Zhu, L.; Peng, W.L.; He, X.C.; Chen, H.L.; Li, J.; Yu, T.; Liang, Z.T.; Zhao, Z.Z.; Chen, H.B. Comparison of ten major constituents in seven types of processed tea using HPLC-DAD-MS followed by principal component and hierarchical cluster analysis. *LWT—Food Sci. Technol.* **2015**, *62*, 194–201. [CrossRef]
37. Li, Z.; Zhu, Y. Surface-modification of SiO_2 nanoparticles with oleic acid. *Appl. Surf. Sci.* **2003**, *211*, 315–320. [CrossRef]